INTERNATIONAL JOURNAL FOR NUMERICAL METHODS IN FLUIDS
Int. J. Numer. Meth. Fluids 2010; **63**:449–467
Published online 23 June 2009 in Wiley InterScience (www.interscience.wiley.com). DOI: 10.1002/fld.2083

Discontinuous Galerkin solution of preconditioned Euler equations for very low Mach number flows

A. Nigro[1], C. De Bartolo[1,*,†], R. Hartmann[2] and F. Bassi[3]

[1]*Dipartimento di Meccanica, Università della Calabria, Ponte P. Bucci cubo 44/C, 87036 Rende (CS), Italy*
[2]*Institute of Aerodynamics and Flow Technology, German Aerospace Center (DLR), Lilienthalplatz 7, 38108 Braunschweig, Germany*
[3]*Dipartimento di Ingegneria Industriale, Università di Bergamo, viale Marconi 5, 24044 Dalmine (BG), Italy*

SUMMARY

In this work we present a discontinuous Galerkin (DG) method designed to improve the accuracy and efficiency of the steady-state solution at very low Mach number flows using an explicit scheme. The algorithm is based on a perturbed formulation of the compressible Euler equations and employs the preconditioning of both the instationary term of the governing equations and the dissipative term of the numerical flux function (full preconditioning approach).

The performance of the scheme is demonstrated by solving an inviscid flow past a NACA0012 airfoil at different very low Mach numbers using various degrees of polynomial approximation. We present numerical results computed with and without perturbed variables, which illustrate the influence of the cancellation errors on both the convergence and the accuracy of the DG solutions at low Mach numbers.

Received 12 September 2008; Revised 1 April 2009; Accepted 1 April 2009

KEY WORDS: discontinuous Galerkin finite element method; low Mach number; cancellation error; preconditioning; Euler equations; higher-order numerical scheme

1. INTRODUCTION

Discontinuous Galerkin (DG) methods have received more and more attention in the last years because of their appealing features that justify the widespread application of these methods. In particular, the minimal amount of numerical dissipation and the potential to reduce the gridding requirements and the time necessary to achieve a desired accuracy level of DG solutions make this method very appealing for low Mach number flow computations [1, 2].

*Correspondence to: C. De Bartolo, Dipartimento di Meccanica, Università della Calabria, Ponte P. Bucci cubo 44/C, 87036 Rende (CS), Italy.
†E-mail: c.debartolo@unical.it

The difficulty in solving the compressible Euler equations at low Mach number is due to the large disparity of wave speeds. The well known, undesirable effects of low-speed flow on most numerical schemes include low convergence speed and loss of accuracy, [3–5]. Another issue related to the numerical solution of low-speed flows concerns the careful implementation of non-reflecting boundary conditions [6–8].

Several preconditioning techniques, applied to the governing equations and to their discretizations, have been developed in the past to cope with the stiffness and accuracy problems [6, 9–11]. These techniques basically scale the wave speeds to the same order of magnitude premultiplying the time derivative terms of the governing equations by a preconditioning matrix. For the large family of upwind schemes, preconditioning enters also in the formulation of numerical flux functions in order to properly balance the artificial dissipation implied by the numerical flux formulation, [4, 5, 12]. Some of the most recognized local preconditioners for inviscid and viscous flows were proposed by Turkel [9, 10], Lee and van Leer [11], Weiss and Smith [13] and Choi and Merkle [14].

Recently, Nigro in [15, 16] introduced the low Mach number preconditioning for DG discretizations and reported for Mach numbers down to $M = 10^{-3}$ that the preconditioning technique results in a significant improvement of the convergence speed. Furthermore, it has been shown that the preconditioning enhances the accuracy of numerical solutions.

Nevertheless, it is difficult or impossible to solve Euler equations at very low Mach numbers even with preconditioning. This is due to cancellation errors that occur as an accumulation effect of round-off errors. Round-off errors depend mainly on the floating point representation used and are thus unavoidable.

The problem of the cancellation error can be minimized by formulating the governing equations in terms of perturbed variables [17, 18]. Reference quantities are introduced in the equations for the thermodynamic variables and the computations are performed for the fluctuations.

The governing equations are unaltered and the method can be used in conjunction with standard numerical strategies, like preconditioning. Several previous studies [14, 19–22] showed that this problem can be alleviated by employing the concept of gauge pressure, in which the pressure is decomposed into a constant reference pressure and a relative pressure. Sesterhenn *et al.* [17] extended the relative treatment to all variables and flux vectors. Nevertheless, Lee [23] showed that this approach produced a slight improvement in the convergence process of the energy equation, while the precision of floating-point variables was a much more important factor in the calculations of the temperature field at very low Mach numbers. Usually, double precision allows to circumvent the problem of cancellation errors for engineering accuracy. Notwithstanding, this floating point representation cannot be sufficient to obtain higher accurate results: the higher the accuracy of solution, the larger the number of computations with round-off error occurring at each computation. Thus, the perturbed formulation of the governing equations becomes mandatory to obtain a highly accurate representation of the unknowns at low Mach numbers using higher-order schemes.

Finally, concerning the set of dependent variables, it has been shown in [24] that the conservative incompressible formulation is well defined only for the entropy variables and the primitive variables including pressure. It has also been shown that these two sets of variables are best suited for solving practical problems, with the primitive variables being more accurate than the entropy variables for low speed and incompressible flow computations. For these reasons the primitive variables are often preferred for low Mach number computations [13, 14, 23, 25] and they have also been used to develop numerical schemes well suited for both compressible and incompressible flows.

In this paper we present a preconditioned DG discretization of the two-dimensional compressible Euler equations suitable to compute inviscid very low Mach number flows. The preconditioning

DOI: 10.1002/fld

affects both the time derivative terms of the governing equations, through the action of the Weiss and Smith preconditioning matrix [13], and the numerical dissipation of Roe's Riemann solver used to compute the numerical flux (full preconditioning technique). The method is applicable only to steady-state simulations as the preconditioning of the unsteady terms destroys the time accuracy of the governing equations. The conservative system of equations is written in terms of perturbed variables and iterated to steady state using an explicit scheme.

This paper aims at giving a contribution on developing a conservative DG scheme that is suitable for compressible and incompressible flows. In particular, here we extend the DG discretization of the Euler equations, written in the most appropriate set of primitive variables, to the incompressible limit, we consider the relationships between convergence characteristics and the Mach number for different degrees of polynomial approximation, and, finally, we examine the influence of the cancellation error on both the accuracy of solutions and the convergence characteristics, taking into account the effect of the polynomial degree.

The outline of the paper is as follows. In Section 2 we present the preconditioned form of the compressible Euler equations using primitive variables and perturbed variables. In Section 3 we describe the DG discretization of the governing equations, the boundary conditions and the preconditioned numerical flux function. In Section 4 we give some details on the explicit time-stepping scheme. The performance of the numerical scheme is then demonstrated in Section 5 by computing an inviscid flow around a NACA0012 airfoil for different very low Mach numbers (down to $M=10^{-15}$) and different degrees of polynomial approximation ($P=1,2,3$). Finally, a few conclusions are drawn in Section 6.

2. GOVERNING EQUATIONS

2.1. The preconditioned compressible Euler equations

We consider the preconditioned two-dimensional compressible Euler equations in conservative form as

$$\mathbf{\Gamma}\frac{\partial \mathbf{q}}{\partial t}+\nabla\cdot\mathbf{F}=0 \tag{1}$$

The primitive variables $\mathbf{q}$ and the cartesian components $\mathbf{f}$ and $\mathbf{g}$ of the flux function $\mathbf{F}$ are given by

$$\mathbf{q}=\begin{pmatrix} p \\ u \\ v \\ T \end{pmatrix}, \quad \mathbf{f}=\begin{pmatrix} \rho u \\ \rho u^2+p \\ \rho uv \\ \rho Hu \end{pmatrix}, \quad \mathbf{g}=\begin{pmatrix} \rho v \\ \rho vu \\ \rho v^2+p \\ \rho Hv \end{pmatrix} \tag{2}$$

where p is the pressure, T is the fluid temperature, u and v are the velocity components, ρ is the density and H is the total enthalpy per unit mass. By assuming that the fluid obeys the perfect gas state equation, H is given by $H=c_pT+0.5(u^2+v^2)$, where c_p denotes the isobaric specific heat capacity of the fluid, and ρ can be calculated as $\rho=p/T$.

DOI: 10.1002/fld

The matrix $\mathbf{\Gamma}$ used in the present work is the local preconditioning matrix of Weiss and Smith [13] written in the following form:

$$\mathbf{\Gamma}=\begin{pmatrix} \Theta & \rho_T & 0 & 0 \\ \Theta u & \rho_T u & \rho & 0 \\ \Theta v & \rho_T v & 0 & \rho \\ \Theta H-1 & \rho_T H+\rho c_p & \rho u & \rho v \end{pmatrix} \tag{3}$$

where $\rho_T=\partial\rho/\partial T|_{p=\text{const.}}$ and Θ is given by

$$\Theta=\left(\frac{1}{U_{\text{r}}^2}-\frac{\rho_T}{\rho c_p}\right) \tag{4}$$

Here, U_{r} is a reference velocity which, for an ideal gas, is defined as

$$U_{\text{r}}=\begin{cases} \varepsilon c & \text{if } |\mathbf{v}|<\varepsilon c \\ |\mathbf{v}| & \text{if } \varepsilon c<|\mathbf{v}|<c \\ c & \text{if } |\mathbf{v}|>c \end{cases} \tag{5}$$

where c is the acoustic speed and ε is a small number included to prevent singularities at stagnation points. Furthermore, by assuming that the fluid obeys the perfect gas state equation, ρ_T can be calculated as $\rho_T=-\rho/T$. Choosing $\varepsilon=O(M)$, the low Mach preconditioning ensures that the convective and acoustic wave speeds are of similar magnitude, proportional to the flow speed [26].

In the next section we will show how preconditioning enters in the formulation of the numerical flux function in the normal direction at Gauss integration points on inter-element faces. Hence, it is worthwhile introducing here the wave speeds of the preconditioned Euler equations in the direction of the unit vector $\mathbf{n}$, which are given by the eigenvalues of $\mathbf{\Gamma}^{-1}((\partial\mathbf{f}/\partial\mathbf{q})n_1+(\partial\mathbf{g}/\partial\mathbf{q})n_2)$, where $\partial\mathbf{f}/\partial\mathbf{q}$ and $\partial\mathbf{g}/\partial\mathbf{q}$ are the inviscid flux Jacobians with respect to the primitive variables, and n_1 and n_2 are the components of the unit vector $\mathbf{n}=(n_1,n_2)^{\text{T}}$. The propagation speeds in this direction are

$$\lambda_1=\lambda_2=u_n, \quad \lambda_3=u_n'+c', \quad \lambda_4=u_n'-c'$$

where

$$\begin{aligned} u_n &= \mathbf{v}\cdot\mathbf{n} \\ u_n' &= u_n(1-\alpha) \\ c' &= \sqrt{\alpha^2 u_n^2+U_{\text{r}}^2} \\ \alpha &= \frac{1-\beta U_{\text{r}}^2}{2} \\ \beta &= \left(\rho_p+\frac{\rho_T}{\rho c_p}\right) \\ \rho_p &= \left.\frac{\partial\rho}{\partial p}\right|_{T=\text{const.}} \end{aligned} \tag{6}$$

DOI: 10.1002/fld

For an ideal gas $\rho_p = 1/T$ and $\beta = 1/c^2$. At low speed as $U_r \to 0$, $\alpha \to \frac{1}{2}$, and all the eigenvalues become of the same order as u_n. We note that all the above equations have been written in non-dimensional form using the dimensional relationships with the reference values of length l_r, density ρ_r, pressure p_r and gas constant R_r. The non-dimensionalized quantities have the following orders of magnitude:

$$\begin{aligned} &p, \rho, T \sim O(1), \quad u, v, u_n \sim O(M), \quad H, c_p \sim O(1) \\ &u_n', c' \sim O(M), \quad \Theta \sim O(M^{-2}) \end{aligned} \tag{7}$$

2.2. Perturbed variables

In this work the relative thermodynamic dependent variables p' and T' are defined as

$$\begin{aligned} p' &= p - p_\infty \\ T' &= T - T_\infty \end{aligned} \tag{8}$$

where p_∞ and T_∞ are the freestream pressure and temperature, respectively. Furthermore, the momentum fluxes are defined considering the relative pressure, p'. Then the primitive variables $\mathbf{q}$ and the cartesian components $\mathbf{f}$ and $\mathbf{g}$ of the convective flux function $\mathbf{F}$ are given as follows:

$$\mathbf{q} = \begin{bmatrix} p' \\ u \\ v \\ T' \end{bmatrix}, \quad \mathbf{f} = \begin{bmatrix} \rho u \\ \rho u u + p' \\ \rho u v \\ \rho H u \end{bmatrix}, \quad \mathbf{g} = \begin{bmatrix} \rho v \\ \rho v u \\ \rho v v + p' \\ \rho H v \end{bmatrix} \tag{9}$$

The perturbed formulation of the preconditioned governing equations obtained using Equation (9) is mathematically equivalent to the original one, Equation (1). In particular, the preconditioning matrix, Equation (3), is not modified and the ideal gas law is maintained.

3. THE PRECONDITIONED DG DISCRETIZATION

Multiplying Equation (1) by a vector-valued test function $\mathbf{v}$ and integrating by parts, we obtain the weak formulation

$$\int_\Omega \mathbf{v}^{\mathrm{T}} \boldsymbol{\Gamma} \frac{\partial \mathbf{q}}{\partial t} \, \mathrm{d}\mathbf{x} - \int_\Omega \nabla \mathbf{v}^{\mathrm{T}} \cdot \mathbf{F} \, \mathrm{d}\mathbf{x} + \int_{\partial\Omega} \mathbf{v}^{\mathrm{T}} \mathbf{F} \cdot \mathbf{n} \, \mathrm{d}s = 0 \quad \forall \mathbf{v} \in H^1(\Omega) \tag{10}$$

where Ω is the domain with boundary $\partial\Omega$ and $\mathbf{n}$ is the unit outward normal vector. To discretize in space, we define $\mathbf{V}_h^p$ to be the space of discontinuous vector-valued polynomials of degree p on a subdivision T_h of the domain into non-overlapping elements such that $\Omega = \bigcup_{\kappa \in T_h} \kappa$. Thus, the solution and test function space is defined by

$$\mathbf{V}_h^p = \{\mathbf{v} \in L^2(\Omega) \ \mathbf{v}|_\kappa \in P_p, \kappa \in T_h\}$$

DOI: 10.1002/fld

where P_p is the space of polynomial functions of degree at most p. The discrete problem then takes the following form: find $\mathbf{q}_h \in \mathbf{V}_h^p$ such that

$$\sum_{\kappa \varepsilon T_h} \left\{ \int_\kappa \mathbf{v}_h^{\mathrm{T}} \boldsymbol{\Gamma} \frac{\partial \mathbf{q}_h}{\partial t} \,\mathrm{d}\mathbf{x} - \int_\kappa \nabla \mathbf{v}_h^{\mathrm{T}} \cdot \mathbf{F}(\mathbf{q}_h) \,\mathrm{d}\mathbf{x} + \int_{\partial\kappa \setminus \partial\Omega} \mathbf{v}_h^{+^{\mathrm{T}}} \mathbf{H}_i(\mathbf{q}_h^+, \mathbf{q}_h^-, \mathbf{n}) \,\mathrm{d}s + \int_{\partial\kappa \cap \partial\Omega} \mathbf{v}_h^{+^{\mathrm{T}}} \mathbf{H}_b(\mathbf{q}_h^+, \mathbf{q}_h^b, \mathbf{n}) \,\mathrm{d}s \right\} = 0 \tag{11}$$

for all $\mathbf{v}_h \in \mathbf{V}_h^p$, where $\mathbf{H}_i(\mathbf{q}_h^+, \mathbf{q}_h^-, \mathbf{n})$ and $\mathbf{H}_b(\mathbf{q}_h^+, \mathbf{q}_h^b, \mathbf{n})$ are numerical flux functions defined on interior and boundary faces, respectively. $\mathbf{H}_i$ takes into account the possible discontinuities of $\mathbf{q}_h$ at element interfaces. On interior edges $\partial\kappa \setminus \partial\Omega$, $\mathbf{H}_i$ depends on the elements interior state $\mathbf{q}_h^+$ and on the neighboring elements state $\mathbf{q}_h^-$. On boundary edges $\partial\kappa \cap \partial\Omega$, $\mathbf{H}_b$ depends on the interior state $\mathbf{q}_h^+$ and a consistent boundary state $\mathbf{q}_h^b$. We note that $\mathbf{H}_b$ may be different from $\mathbf{H}_i$.

Given a set of basis functions ψ_j, $j = 1, \ldots, N$, of the discrete function space $\mathbf{V}_h^p$ with $N = \#\mathbf{V}_h^p$ we define the residual vector $\mathbf{R} = \{(\mathscr{R}(\mathbf{q}_h), \psi_j)\}_{j=1,\ldots,N}$, where

$$(\mathscr{R}(\mathbf{q}_h), \mathbf{v}_h) \equiv \int_\kappa \nabla \mathbf{v}_h^{\mathrm{T}} \cdot \mathbf{F}(\mathbf{q}_h) \,\mathrm{d}\mathbf{x} - \int_{\partial\kappa \setminus \partial\Omega} \mathbf{v}_h^{+^{\mathrm{T}}} \mathbf{H}_i(\mathbf{q}_h^+, \mathbf{q}_h^-, \mathbf{n}) \,\mathrm{d}s - \int_{\partial\kappa \cap \partial\Omega} \mathbf{v}_h^{+^{\mathrm{T}}} \mathbf{H}_b(\mathbf{q}_h^+, \mathbf{q}_h^b, \mathbf{n}) \,\mathrm{d}s$$

for all $\mathbf{v}_h \in \mathbf{V}_h^p$. Then the spatial DG discretization of Equation (11) results in the following global system of equations:

$$\mathbf{M}_\Gamma \frac{\mathrm{d}\mathbf{Q}}{\mathrm{d}t} - \mathbf{R} = 0 \tag{12}$$

where $\mathbf{Q}$ is the global vector of degrees of freedom (dof) with $\mathbf{q}_h = \sum_{j=1,\ldots,N} Q_j \psi_j$. $\mathbf{R}$ is the residual vector as defined above and $\mathbf{M}_\Gamma$ stands for the discretization of the first integral of Equation (11). Hence, $\mathbf{M}_\Gamma$ is a block diagonal matrix where the block corresponding to one element couples all the dof of all variables within the element (the coupling among dof of different variables is due to the action of $\boldsymbol{\Gamma}$).

3.1. Boundary conditions

When $\partial\kappa$ belongs to $\partial\Omega$ the boundary fluxes, denoted by $\mathbf{H}_b(\mathbf{q}^+, \mathbf{q}^b, \mathbf{n})$, are chosen to weakly prescribe the boundary conditions of the problem. Here, $\mathbf{n}$ is the unit outward normal vector, $\mathbf{q}^+$ is the interior state at the boundary and $\mathbf{q}^b$ is computed according to the conditions that must be satisfied on the boundary.

At far field, $\mathbf{H}_b$ is the numerical flux function $\mathbf{H}_i(\mathbf{q}^+, \mathbf{q}^b, \mathbf{n})$, where $\mathbf{q}^b$ is computed by imposing a set of simplified non-reflecting boundary conditions [6] to minimize spurious reflections. In particular at the inflow boundary, the state $\mathbf{q}^b$ has the same pressure as $\mathbf{q}^+$, whereas the velocity vector and the temperature are prescribed based on the freestream values. Conversely, at the outflow boundary, the state $\mathbf{q}^b$ has the same temperature and velocity vector as $\mathbf{q}^+$, whereas the pressure is prescribed based on the freestream value. We remark that the simplified non-reflecting boundary conditions require a far-field boundary well far away from the aerodynamic surface in order to get efficient and accurate solutions.

At solid walls, $\mathbf{H}_b$ is the inviscid flux function in the direction normal to the wall $\mathbf{F}(\mathbf{q}^b) \cdot \mathbf{n}$, where $\mathbf{q}^b$ has the same pressure and temperature as $\mathbf{q}^+$, whereas the velocity vector $\mathbf{v}^b = \mathbf{v}^+ - (\mathbf{v} \cdot \mathbf{n})^+ \mathbf{n}$ ensures that the normal velocity component is zero on the boundary, $(\mathbf{v} \cdot \mathbf{n})^b = 0$.

DOI: 10.1002/fld

3.2. Flux difference splitting

The numerical flux $\mathbf{H}_i(\mathbf{q}^+, \mathbf{q}^-, \mathbf{n})$ appearing in Equation (11) is computed based on a preconditioning of the artificial dissipation term of Roe's approximate Riemann solver [27]. In terms of primitive quantities $\mathbf{q}$, the value of $\mathbf{H}_i$ at each face is given by

$$\mathbf{H}_i(\mathbf{q}^+, \mathbf{q}^-, \mathbf{n}) = \tfrac{1}{2}(\mathbf{F}(\mathbf{q}^+)\cdot\mathbf{n} + \mathbf{F}(\mathbf{q}^-)\cdot\mathbf{n} - \tilde{\mathbf{F}}_\Gamma(\mathbf{q}^+, \mathbf{q}^-, \mathbf{n})) \tag{13}$$

where $\tilde{\mathbf{F}}_\Gamma$ is given by

$$\tilde{\mathbf{\Gamma}}|\tilde{\mathbf{A}}_\Gamma|\Delta\mathbf{q} \tag{14}$$

Here, $\Delta\mathbf{q} = \mathbf{q}^- - \mathbf{q}^+$ and the matrix $|\tilde{\mathbf{A}}_\Gamma|$ is defined in terms of the preconditioned eigenvalues and eigenvectors by

$$|\tilde{\mathbf{A}}_\Gamma| = \tilde{\mathbf{T}}_\Gamma|\tilde{\mathbf{\Lambda}}_\Gamma|\tilde{\mathbf{T}}_\Gamma^{-1}$$

The symbol $\tilde{}$ denotes that the matrices are computed using the Roe-averaged variables [28] and the subscript Γ denotes that the diagonal matrix of eigenvalues and the modal matrix are derived from the preconditioned system, where $\tilde{\mathbf{\Lambda}}_\Gamma$ is the diagonal matrix of the preconditioned eigenvalues, and $\tilde{\mathbf{T}}_\Gamma$ diagonalizes the matrix $\tilde{\mathbf{\Gamma}}^{-1}(\widetilde{(\partial\mathbf{F}/\partial\mathbf{q})\cdot\mathbf{n}})$. We note, that for the non-preconditioned system, Equation (13) reduces to the standard Roe's flux difference splitting.

4. TIME DISCRETIZATION OF THE PRECONDITIONED EULER EQUATIONS

The semi-discrete system Equation (12) is discretized in time based on an explicit multistage time-stepping method. In order to overcome the restrictive explicit CFL stability limit (the Courant number is approximately equal to $1/(2p+1)$ for linear stability of TVD Runge–Kutta schemes, where p is the polynomial degree of the spatial discretization), both the local time stepping and the preconditioning techniques have been used to improve the convergence speed to steady-state solutions.

The solution is advanced from time t to time $t+\Delta t$ with an s-stage SSP Runge–Kutta scheme [29], given by

$$\begin{aligned}
\mathbf{Q}^0 &= \mathbf{Q}^t \\
\mathbf{Q}^i &= \sum_{k=0}^{i-1} \alpha_{ik}\mathbf{Q}^k + \beta_{ik}\Delta t\mathbf{M}_\Gamma^{-1}\mathbf{R}(\mathbf{Q}^k), \quad i = 1, 2, \ldots, s \\
\mathbf{Q}^{t+\Delta t} &= \mathbf{Q}^s
\end{aligned} \tag{15}$$

where i is the stage counter for the s-stage scheme and α_{ik} and β_{ik} are the multistage coefficients for the ith stage.

The local time step Δt on each element κ is computed by considering the following relation:

$$\Delta t = \frac{\sigma}{2p+1}\cdot\frac{|\kappa|}{\Lambda_c^x + \Lambda_c^y} \tag{16}$$

DOI: 10.1002/fld

where the preconditioned convective spectral radii Λ_c^x and Λ_c^y are defined as

$$\begin{aligned} \Lambda_c^x &= (|\bar{u}'| + \bar{c}_x')\Delta S^x \\ \Lambda_c^y &= (|\bar{v}'| + \bar{c}_y')\Delta S^y \end{aligned} \tag{17}$$

The variables ΔS^x and ΔS^y represent the projections of the element κ onto the x- and y-axis, respectively, whereas $\bar{u}'$, $\bar{c}_x'$ and $\bar{v}'$, $\bar{c}_y'$ are obtained applying Equations (6) along the x and y directions and using the mean values of the flow quantities on each element κ. Finally, p is the polynomial degree of the spatial discretization and σ is a factor introduced to take into account that SSP can be more efficient than TVD Runge–Kutta schemes.

5. RESULTS

In this section, we present some numerical results demonstrating the performance of the proposed preconditioned DG discretization for inviscid very low Mach number flows. To this end, we consider an inviscid flow past a NACA0012 airfoil at zero angle of attack comparing the preconditioned DG discretizations with and without perturbed variables. DG solutions on a triangular O-type grid for different very low Mach numbers and using linear (P_1), quadratic (P_2) and cubic (P_3) elements are performed. Figure 1 shows the computational grid. The grid is composed of 1792 elements, and the far-field boundary is located far away from the aerodynamic surface. All computations are performed in double precision, storing 16 significant digits.

The computational results are organized in two subsections, one focusing on the convergence characteristics of the preconditioned Euler equations and the other on the accuracy of the converged solutions.

The residual histories of pressure, p, temperature, T, horizontal, u, and vertical, v, velocity components versus iteration number are shown to represent the convergence characteristics.

The accuracy of the converged solutions is analyzed both qualitatively and quantitatively. First, the normalized pressure fields are presented for a qualitative comparison. Then, for the quantitative analysis, the scaling of computed pressure fluctuations as the Mach number reduces is compared with the M^2 theoretical scaling.

5.1. Effect of the perturbed variables on convergence characteristics

The residuals are measured in terms of the absolute value of the ratio between the dependent variable changes and the local time step, both computed for each element κ using the mean values of the flow quantities. The residual of the generic dependent variable, q, was defined as:

$$\mathrm{Res}(q) = \mathrm{Max}\{|\Delta(\bar{q})/\Delta t|_\kappa, \forall \kappa \in \Omega\} \quad \text{with } q = p,\, T,\, u,\, v \tag{18}$$

The convergence histories of velocity are represented by the residuals of the horizontal velocity component as similar histories are obtained for the vertical velocity component. Figure 2 shows the convergence characteristics of pressure (left column), temperature (middle column) and velocity (right column) at $M = 10^{-2}$, $M = 10^{-4}$ and $M = 10^{-6}$, for linear (P_1 top row), quadratic (P_2 middle row) and cubic (P_3 bottom row) elements, without the perturbed variables. The residuals are normalized with respect to the residual at the first time step. Overall, we see that, for a given polynomial degree, all the convergence characteristics have the same convergence speed, which

DOI: 10.1002/fld

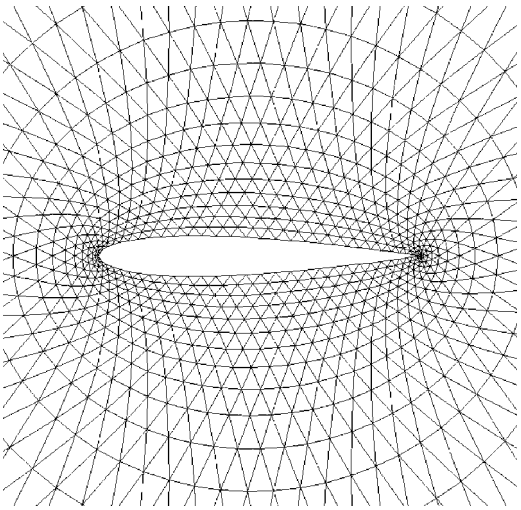

Figure 1. Computational grid.

is independent of the Mach number. Nevertheless, the efficiency of the preconditioned scheme reduces due to the CFL stability condition.

Furthermore in Figure 2 the influence of cancellation error on the residual decay can be clearly seen. Examining the convergence histories of pressure, temperature, and velocity we can make two observations. The first is that, for a given polynomial degree, the lower the Mach number, the smaller the residual decay. The second is that, for a given Mach number, the higher the polynomial degree, the smaller the reduction of the residual, even if this influence is less evident than the first.

However, both the influence of Mach number and polynomial degree on the decrease of the residual did not allowed to obtain a solution at the lowest Mach number $M = 10^{-6}$ using the highest polynomial degree P_3.

Figure 3 shows the convergence characteristics with the perturbed variables. The residuals are not normalized in order to highlight for the dependence of convergence characteristics on the Mach number. We see that all the residuals decrease as the Mach number reduces. Specifically, the convergence of pressure and temperature scale as $O(M^3)$, whereas the residual of velocity scales as $O(M^2)$. Then, as from Equation (16) and Equation (17) the order of magnitude of the local time stepping is $O(M^{-1})$, due to the order given in Equation (7), the resulting orders of magnitude of the computed pressure, temperature and velocity changes are $O(M^2)$, $O(M^2)$ and $O(M)$, respectively, in perfect agreement with the theoretical behavior.

Figure 4 shows the convergence characteristics with the perturbed variables, obtained scaling the residuals of pressure, temperature and velocity as follows:

$$\begin{aligned} \mathrm{Res}(p) &= \mathrm{Max}\left\{\frac{|\Delta\bar{p}/\Delta t|_\kappa}{M^3}, \forall\kappa\in\Omega\right\} \\ \mathrm{Res}(T) &= \mathrm{Max}\left\{\frac{|\Delta\bar{T}/\Delta t|_\kappa}{M^3}, \forall\kappa\in\Omega\right\} \\ \mathrm{Res}(u) &= \mathrm{Max}\left\{\frac{|\Delta\bar{u}/\Delta t|_\kappa}{M^2}, \forall\kappa\in\Omega\right\} \end{aligned} \tag{19}$$

DOI: 10.1002/fld

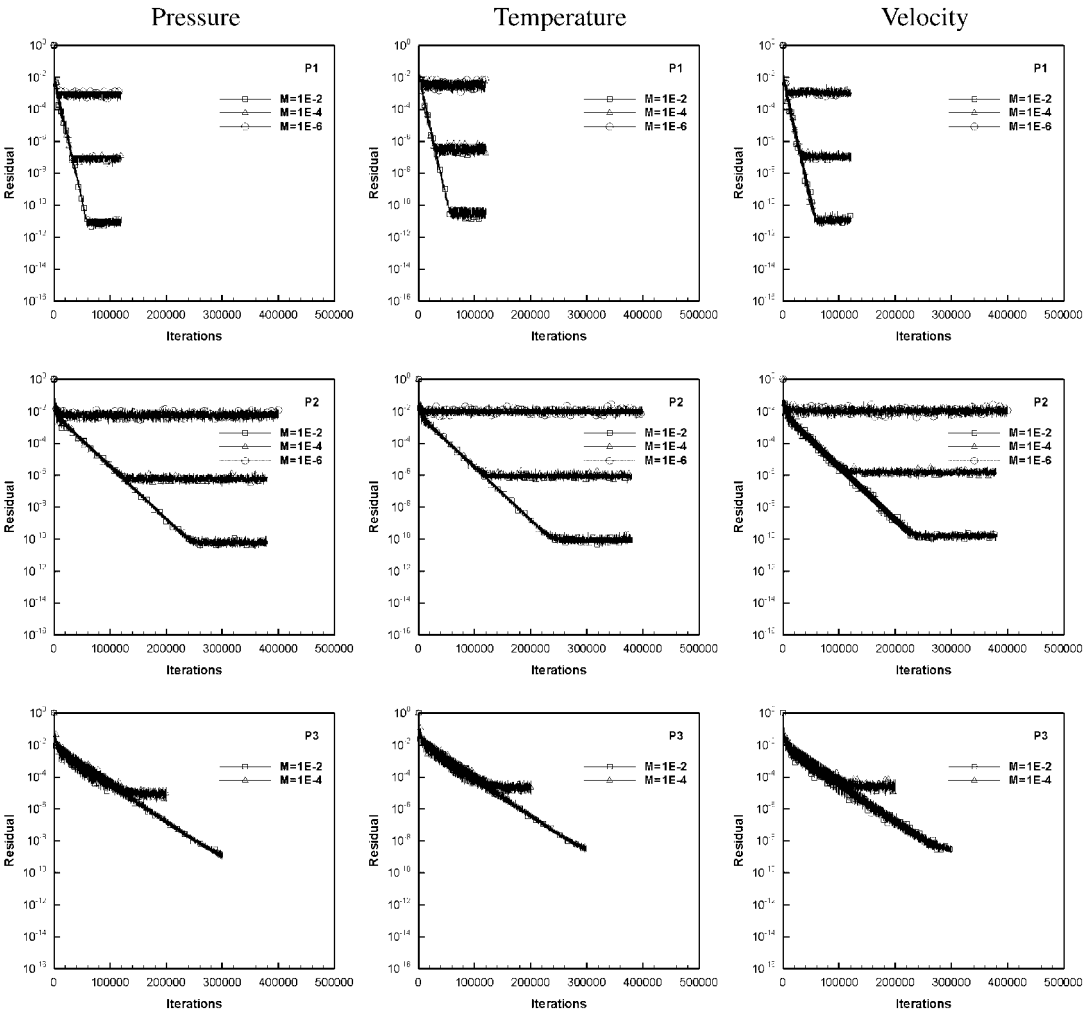

Figure 2. History of the nonlinear residuals versus number of iteration steps for the pressure (left column), temperature (middle column) and velocity (right column), in normalized form without the perturbed variables at $M=10^{-2}$, $M=10^{-4}$ and $M=10^{-6}$. P_1 (top row), P_2 (middle row) and P_3 (bottom row) elements.

The plots show that the perturbed variables do not affect the convergence speed in comparison to the non-perturbed solution (Figure 2). We notice that the residual decay of pressure and velocity are now independent of the Mach number.

The case is different for the temperature. We see that even if we use the perturbed variables, the residual of temperature reduces less as compared with the residual of pressure because they stagnate at a level closer to the starting value. In particular, the decay of the temperature residual strongly reduces when Mach number approaches zero. The reason of this behavior can be found in the order of magnitude of the convective fluxes as the Mach number approaches zero. Owing

DOI: 10.1002/fld

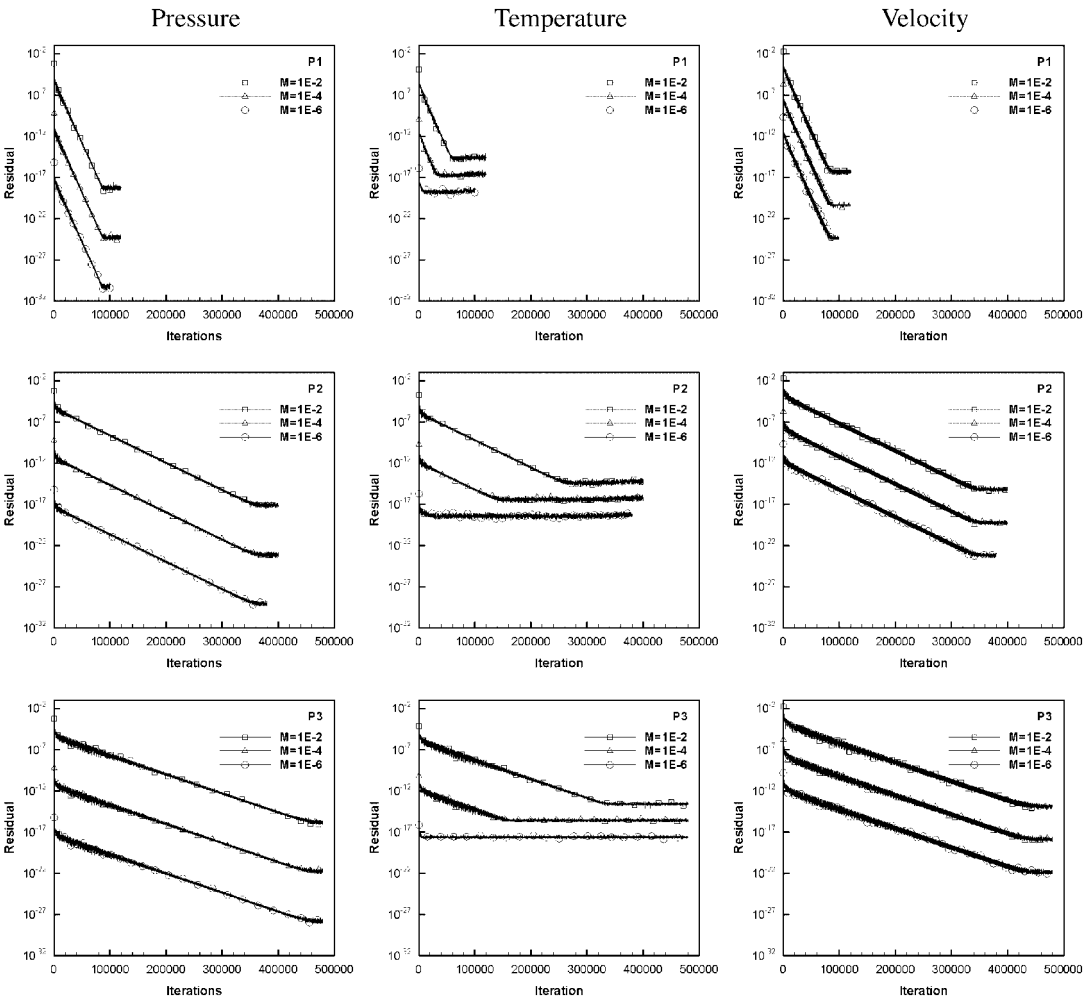

Figure 3. History of the nonlinear residuals versus number of iteration steps for the pressure (left column), temperature (middle column) and velocity (right column), with the perturbed variables at $M=10^{-2}$, $M=10^{-4}$ and $M=10^{-6}$. P_1 (top row), P_2 (middle row) and P_3 (bottom row) elements.

to the orders of magnitude of the non-dimensionalized quantities, Equation (7), and considering that $p' \sim O(M^2)$, the convective fluxes in the x and y direction, Equation (9), can be expressed as follows:

$$\mathbf{f},\mathbf{g} \sim \begin{pmatrix} O(M) \\ O(M^2) \\ O(M^2) \\ O(M)+O(M^3) \end{pmatrix}$$

DOI: 10.1002/fld

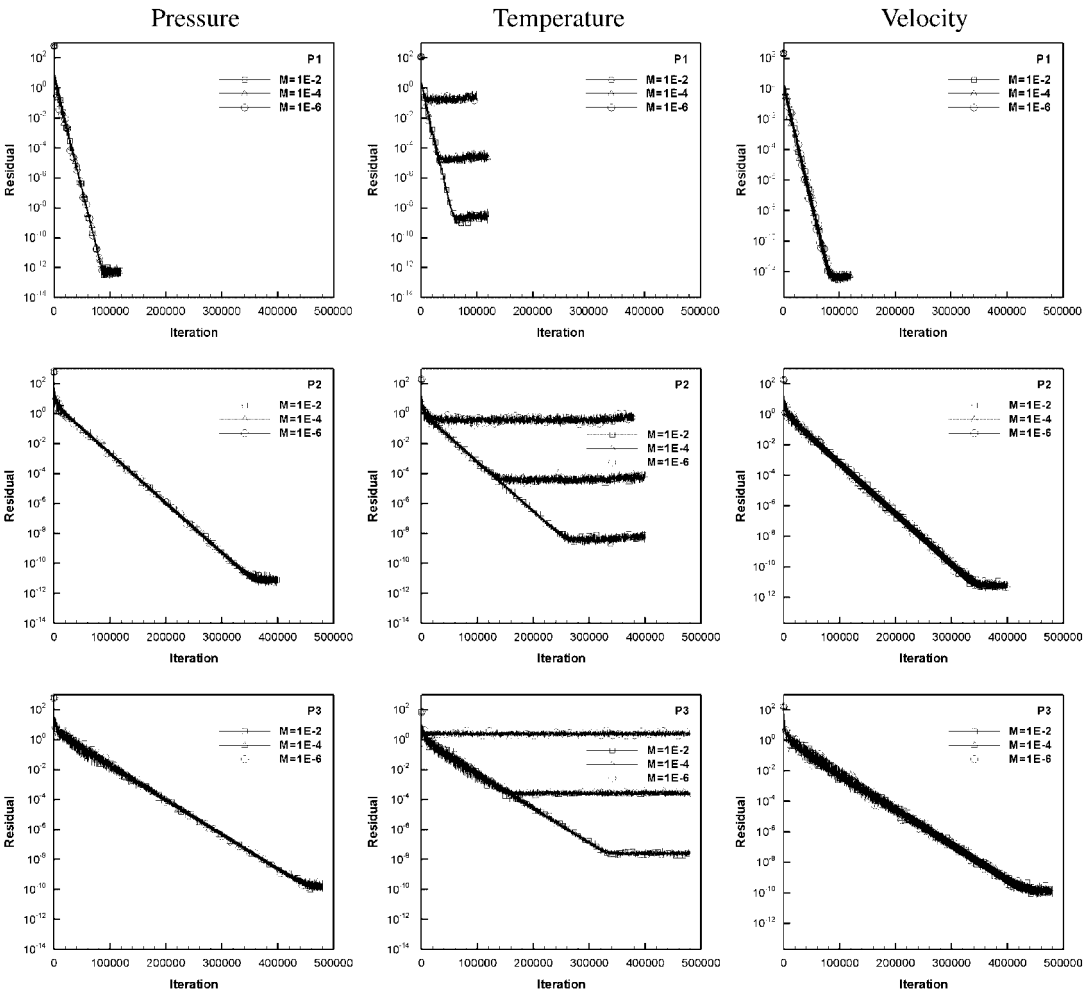

Figure 4. History of the nonlinear residuals versus number of iteration steps for the pressure (left column), temperature (middle column) and velocity (right column), in scaled form with the perturbed variables at $M = 10^{-2}$, $M = 10^{-4}$ and $M = 10^{-6}$. P_1 (top row), P_2 (middle row) and P_3 (bottom row) elements.

We see that the range of the order of magnitude of the flux in the energy equation is wider than that in the other equations. Thereby, the temperature suffers more from the cancellation problem than the other variables [23].

The dependency of the residual reduction on the polynomial degree is the same previously observed without the perturbed variables.

Furthermore, we note that using the perturbed variables, while the residual decay of pressure and velocity is sufficient enough to obtain accurate flow variable distributions, the lowest level of residual reduction of the temperature shows a strong effect of the cancellation error and this not always allowed to compute accurate temperature fields.

DOI: 10.1002/fld

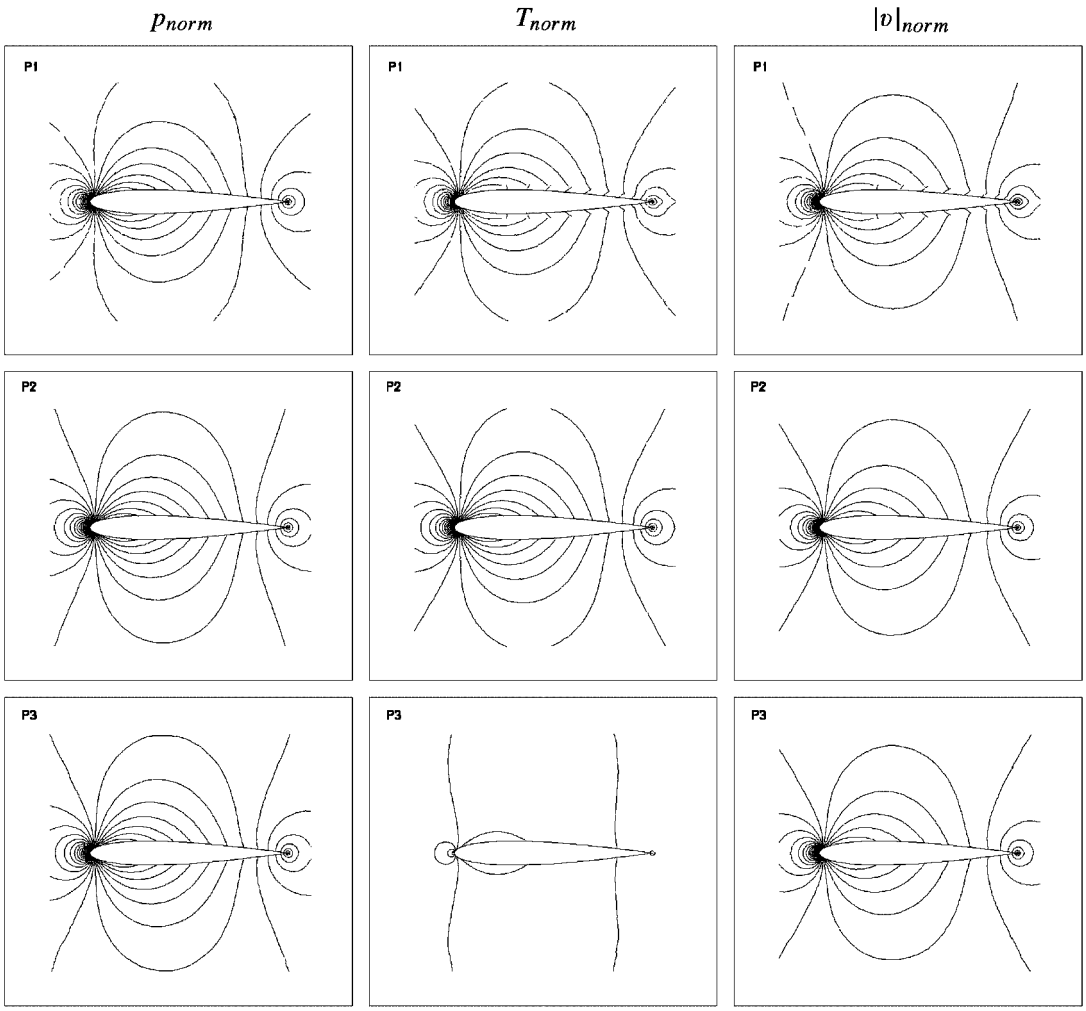

Figure 5. Non-perturbed method: test at $M = 10^{-5}$. Contours of normalized pressure (left column), temperature (middle column) and velocity (right column). P_1 (top row), P_2 (middle row) and P_3 (bottom row) elements.

Finally, we observe that the explicit scheme results in an inefficient solution technique even using preconditioning. This is due to the restrictive limitations on the CFL number for higher-order discretizations. A multigrid strategy might be implemented for the explicit time-stepping scheme in order to accelerate the convergence of the preconditioned Euler equations to the steady-state solution.

5.2. *Effect of the perturbed variables on the solution accuracy*

5.2.1. Normalized isolines. In the following, we present the contour plots of the normalized pressure, p_{norm}, temperature, T_{norm} and absolute value of velocity, $|v|_{\text{norm}}$. The normalized variable,

DOI: 10.1002/fld

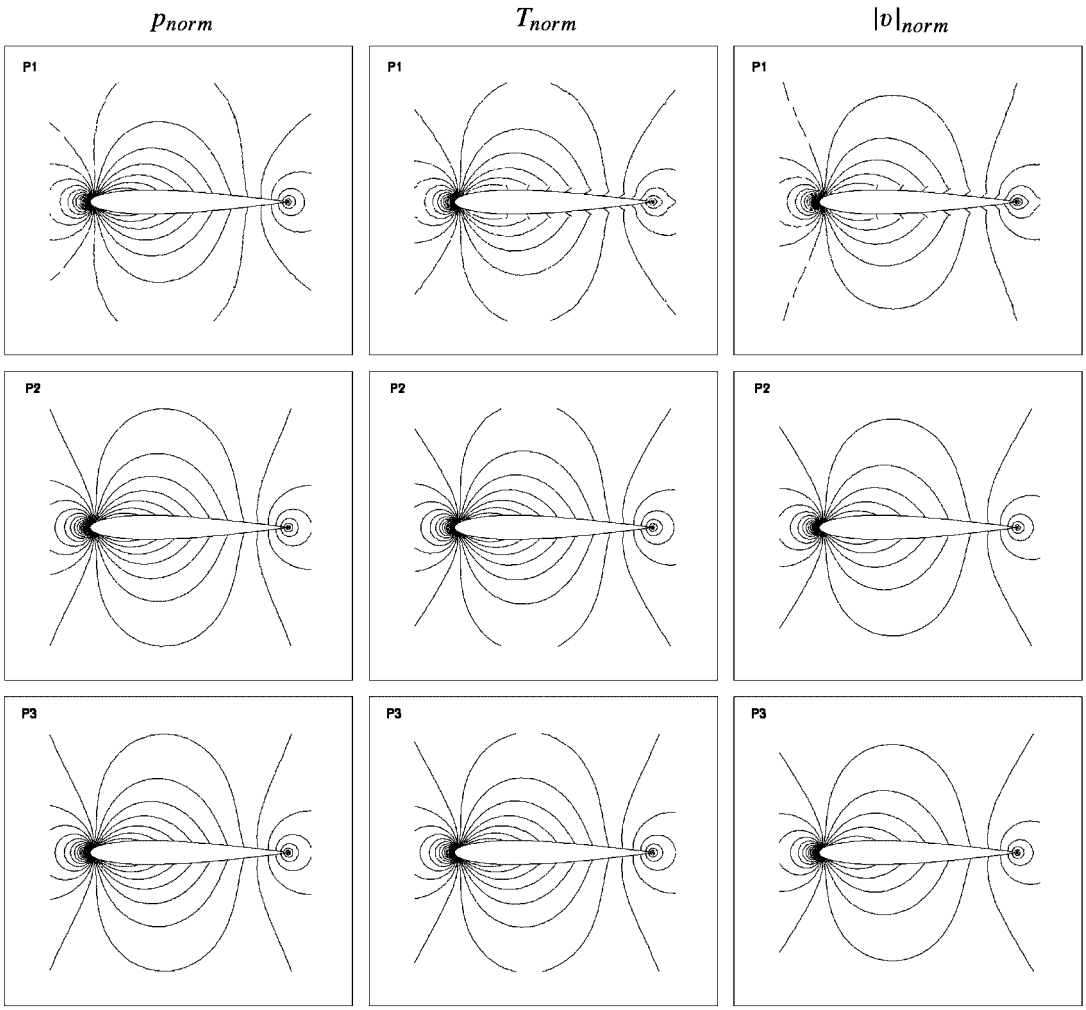

Figure 6. Perturbed method: test at $M = 10^{-5}$. Contours of normalized pressure (left column), temperature (middle column) and velocity (right column). P_1 (top row), P_2 (middle row) and P_3 (bottom row) elements.

q_{norm}, was defined as

$$q_{\text{norm}} = (q - q_{\min})/(q_{\max} - q_{\min})$$

where $q = p, T, |v|$. Figures 5 and 6 show the normalized contours of pressure (left column), temperature (middle column) and velocity vector (right column) at $M = 10^{-5}$, using P_1 (top row), P_2 (middle row) and P_3 (bottom row) elements, without and with the perturbed variables, respectively. We see that on the basis of normalized pressure and absolute value of velocity isolines there is no difference between the perturbed and the non-perturbed solutions, whereas isolines of temperature begin to deteriorate using P_3 elements and non-perturbated variables.

DOI: 10.1002/fld

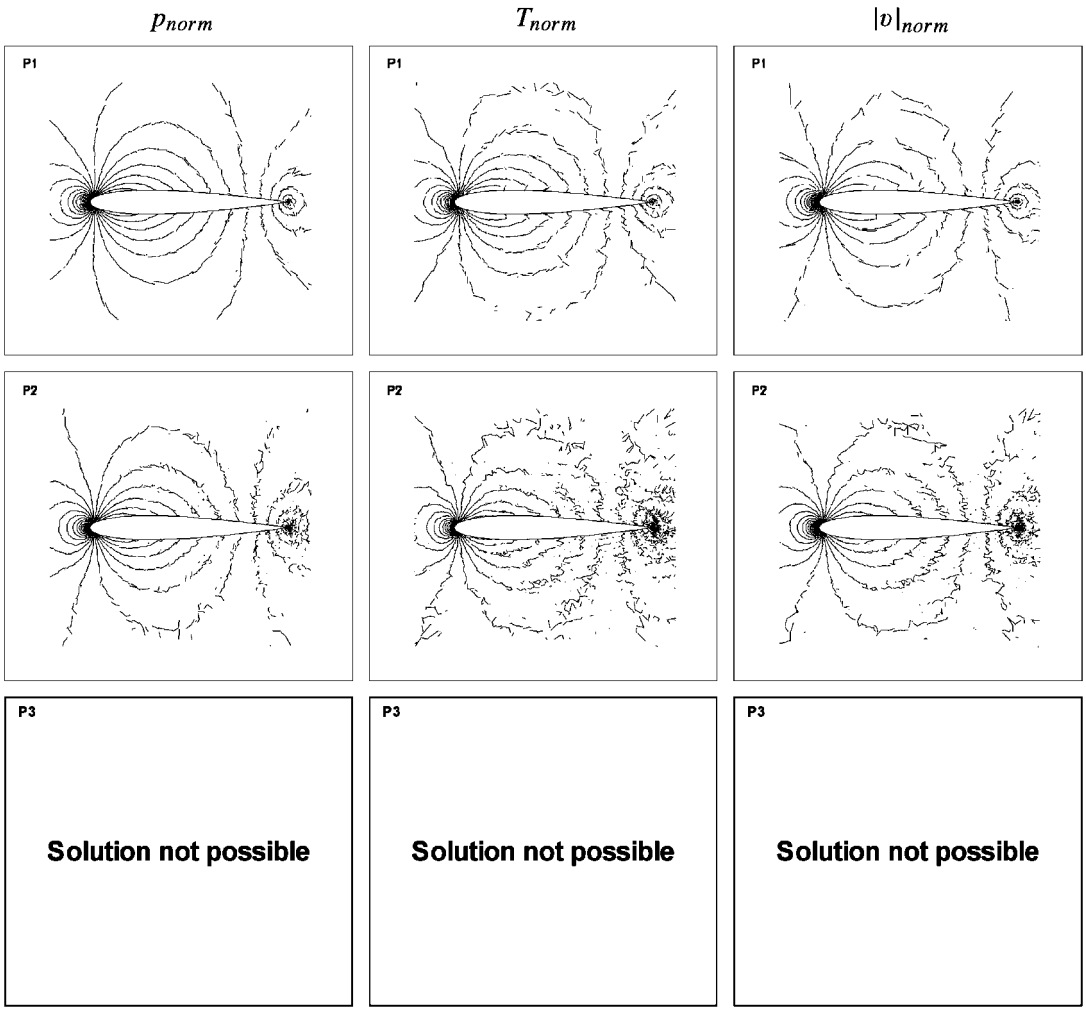

Figure 7. Non-perturbed method: test at $M = 10^{-6}$. Contours of normalized pressure (left column), temperature (middle column) and velocity (right column). P_1 (top row), P_2 (middle row) and P_3 (bottom row) elements.

The solutions at $M = 10^{-6}$, see Figures 7 and 8, show more clearly how using the perturbed variables improves the numerical accuracy in the low Mach number limit. Here, the P_1 solutions obtained using non-perturbated variables exhibit numerical oscillations, and the results worsen as the polynomial degree increases. This is due to the higher number of computations performed when the higher-order approximations are used. In other words, the larger the number of computations with rounding errors occurring at each computation, the worse the solution. Like for the P_3 solution at $M = 10^{-6}$, it was not possible to obtain a converged solution for lower Mach numbers, regardless of the polynomial degree. From these results we see that the perturbed variables are fundamental to obtain convergence of continuity and momentum equations at very low Mach numbers, although

DOI: 10.1002/fld

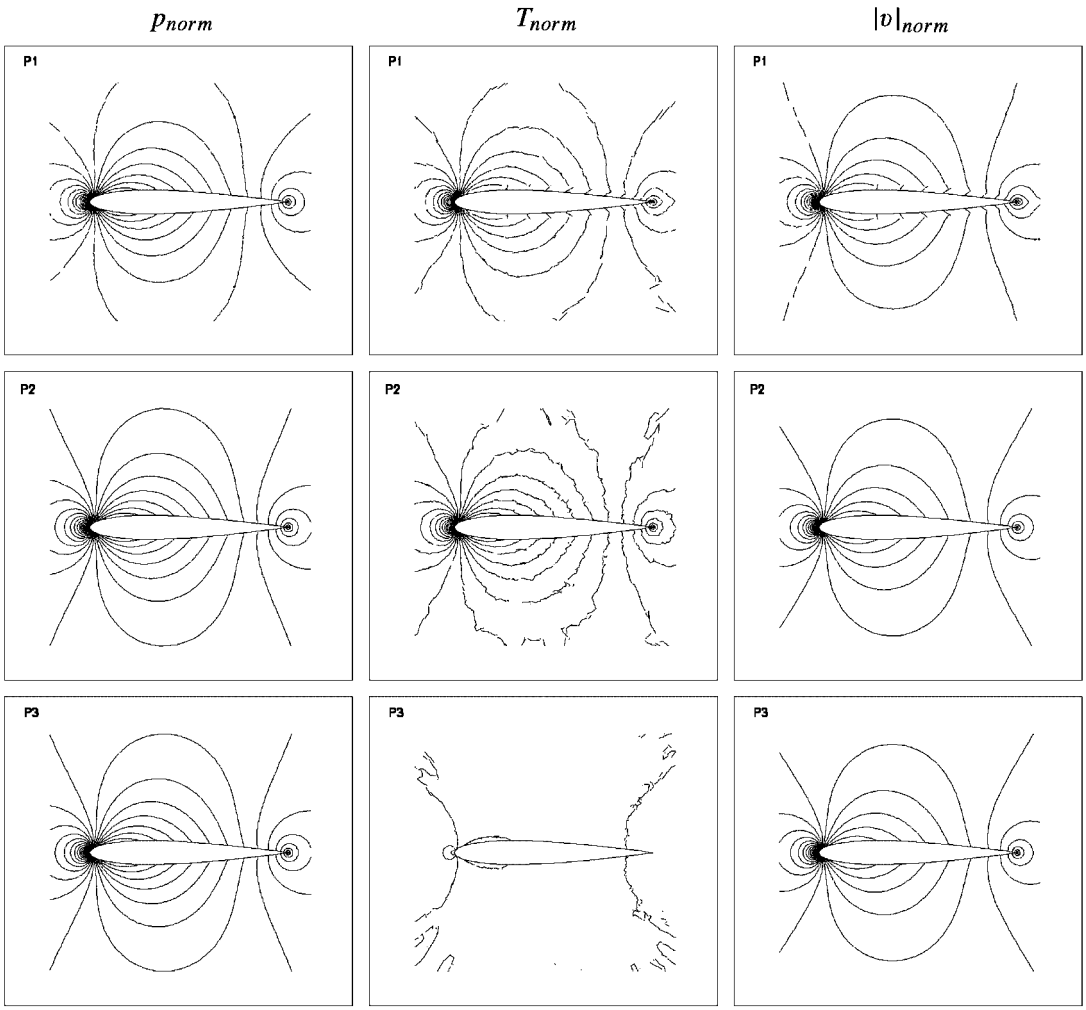

Figure 8. Perturbed method: test at $M = 10^{-6}$. Contours of normalized pressure (left column), temperature (middle column) and velocity (right column). P_1 (top row), P_2 (middle row) and P_3 (bottom row) elements.

the energy equation still does not converge. In fact, the perturbed formulation of the Euler equations allowed to obtain accurate pressure and velocity isolines even for extremely low Mach number adiabatic flows, $M = 10^{-15}$, see Figure 9, independently of the polynomial degree of the numerical solution, thus extending the DG scheme to the incompressible limit.

5.2.2. Pressure fluctuations. Figure 10 shows the pressure fluctuations $(p_{\max} - p_{\min})/p_{\max}$ versus the Mach number at $M = 10^{-2}$, $M = 10^{-4}$, $M = 10^{-6}$ and $M = 10^{-15}$, using P_1, P_2 and P_3 elements, with the perturbed variables. We see that the perturbed formulation of the Euler equations preserves the accuracy of the solutions at extremely low Mach numbers. In perfect agreement with

DOI: 10.1002/fld

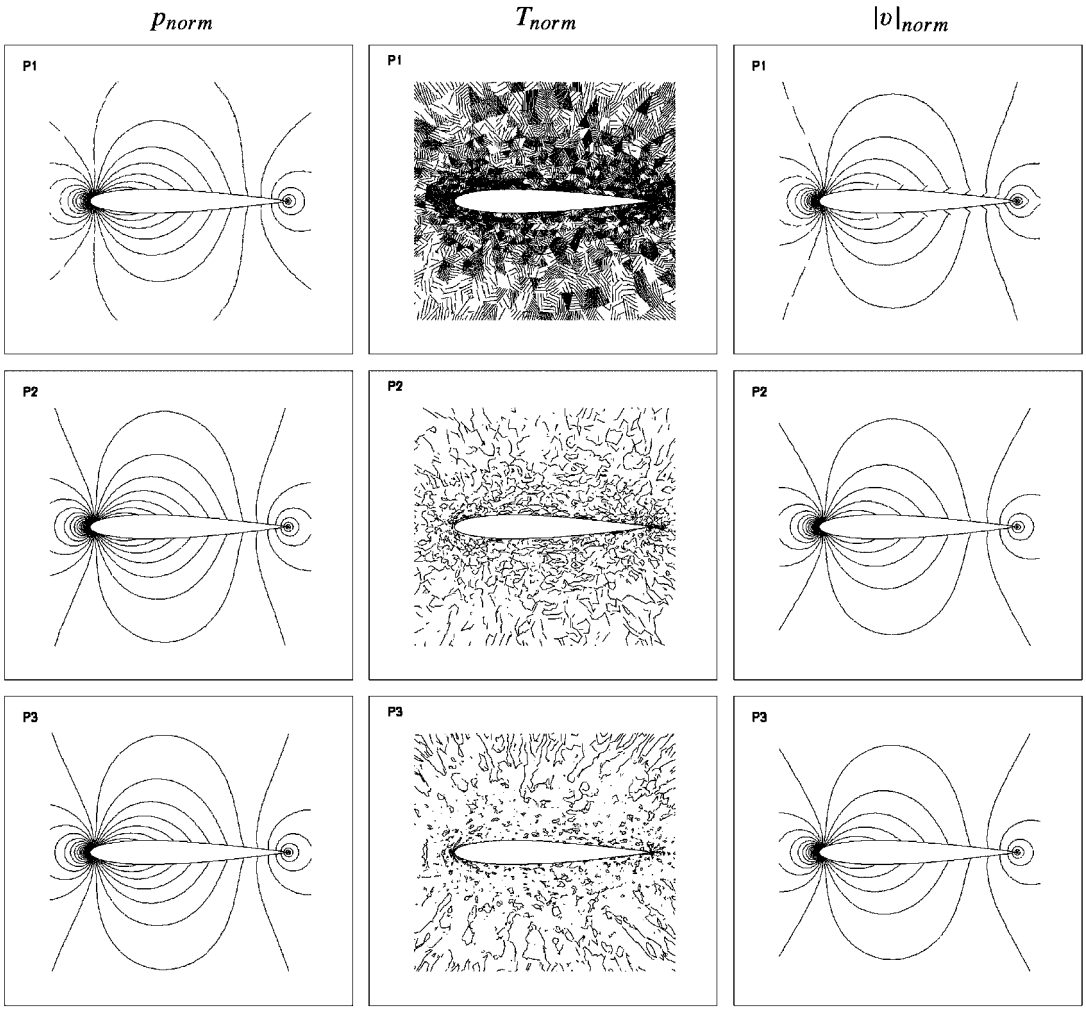

Figure 9. Perturbed method: test at $M = 10^{-15}$. Contours of normalized pressure (left column), temperature (middle column) and velocity (right column). P_1 (top row), P_2 (middle row) and P_3 (bottom row) elements.

the theory, the pressure fluctuations scale exactly with the square of the Mach number down to $M = 10^{-15}$.

6. CONCLUSIONS

In this work we have presented the main features of a preconditioned DG discretization for inviscid very low Mach number computations. The method solves the compressible Euler equations written in terms of primitive variables and iterates to steady-state using an explicit scheme. The algorithm employs the perturbed formulation of the governing equations and the low Mach number

DOI: 10.1002/fld

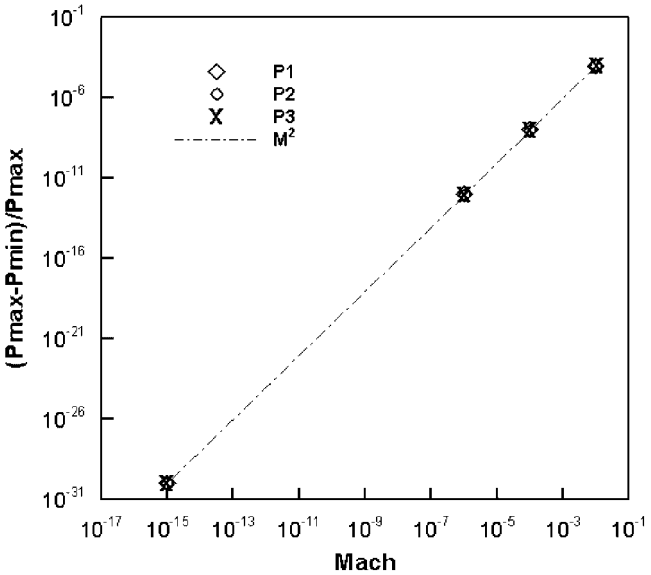

Figure 10. Pressure fluctuations versus Mach number for P_1, P_2 and P_3 elements using perturbed variables. Dashed and dotted line display the theoretical behavior of M^2.

preconditioning of both the time-derivative term of the governing equations and of the numerical flux function (full preconditioning approach).

Numerical results have been presented solving the 2D compressible Euler equations at different very low Mach numbers using linear, quadratic and cubic elements, with and without the perturbed variables. The perturbed formulation allowed to investigate on the relationship between convergence characteristics and Mach number. For a given polynomial degree, the convergence characteristics of continuity, momentum and energy equations were found independent of the Mach number, showing that the scaling of the computed pressure, temperature and velocity changes as Mach number reduces are in agreement with the M^2, M^2 and M theoretical scaling, respectively. Furthermore, for a given Mach number, it was shown that the residual decays reduce when the polynomial degree increases even using perturbed variables. In all cases the convergence speed was not affected by the perturbed variables. Some convergence problems were found for the energy equation at very low Mach numbers due to cancellation errors. Nevertheless, it has been shown that the perturbed formulation is mandatory to obtain accurate pressure and velocity distributions at low Mach numbers, especially when computations are performed using high-order representations of the unknowns.

REFERENCES

1. Luo H, Baum J, Lohner R. A fast *p*-multigrid discontinuous Galerkin method for compressible flows at all speeds. *The 44th AIAA Aerospace Sciences Meeting and Exhibit*, Reno, 2006.
2. Feistauer M, Kucera V. On a robust discontinuous Galerkin technique for the solution of compressible flow. *Journal of Computational Physics* 2007; **224**(1):208–221.
3. Volpe G. Performance of compressible flow codes at low mach numbers. *AIAA Journal* 1993; **31**:49–56.

DOI: 10.1002/fld

4. Turkel E, Fiterman A, vanLeer B. Preconditioning and the limit of the compressible to the incompressible flow equations for finite difference schemes. In *Frontiers of Computational Fluid Dynamics*, Caughey DA, Hafez MM (eds). Wiley: Chichester, 1994; 215–234.
5. Guillard H, Viozat C. On the behavior of upwind schemes in the low mach number limit. *Computers and Fluids* 1999; **28**:63–86.
6. Radespiel R, Turkel E, Kroll N. Assessment of preconditioning methods. *DLR-FB 95-29*, 1995.
7. Moinier P, Giles MB. Compressible Navier–Stokes equations for low mach number applications. *ECCOMAS Computational Fluid Dynamics Conference 2001*, Swansea, Wales, U.K., 4–7 September 2001; 1–14.
8. Muller B. Influence of inlet and outlet boundary conditions in internal flow computations at low mach numbers. In *Computational Fluid Dynamics '96'*, Desideri J-A, Hirsch C, Le Tallec P, Pandolfi M, Periaux J (eds), *Proceedings of the 3rd ECCOMAS CFD Conference*, Paris, 9–13 September 1996. Wiley: Chichester, 1996; 637–643.
9. Turkel E. Review of preconditioning methods for fluid dynamics. *Applied Numerical Mathematics* 1993; **12**: 257–284.
10. Turkel E. Preconditioning techniques in computational fluid dynamics. *Annual Review of Fluid Mechanics* 1999; **31**:385–416.
11. Lee D, VanLeer B. Progress in local preconditioning of the Euler and Navier–Stokes equations. *AIAA Paper 93-3328*, 1993.
12. Lee D. Local preconditioning of the Euler equations and Navier–Stokes equations. *Ph.D. Thesis*, University of Michigan, 1996.
13. Weiss J, Smith WA. Preconditioning applied to variable and constant density flows. *AIAA Journal* 1995; **33**: 2050–2057.
14. Choi YH, Merkle CL. The application of preconditioning in viscous flows. *Journal of Computational Physics* 1993; **105**:207–233.
15. Nigro A. Discontinuous Galerkin methods for inviscid low Mach number flows. *DLR-IB 124-2008/1*, 2008.
16. Bassi F, De Bartolo C, Hartmann R, Nigro A. A discontinuous Galerkin method for inviscid low Mach number flows. *Journal of Computational Physics* 2009; **228**:3996–4011.
17. Sesterhenn J, Muller B, Thomann H. On the cancellation problem in calculating compressible low mach number flow. *Journal of Computational Physics* 1999; **151**:597–615.
18. Muller B, Jenny P. Improving the reliability of low mach number flow computations. *CFD Journal* 2001; **9**(1):518–528.
19. Klein R. Semi-implicit extension of a Godunov-type scheme based on low mach number asymptotycs I: one-dimensional flow. *Journal of Computational Physics* 1995; **121**:213–237.
20. Bijl H, Wesseling P. Unified formulation for compressible and incompressible flows by using multi-intergrated moments II: multi-dimensional version for compressible and incompressible flows. *Journal of Computational Physics* 1998; **141**:153–173.
21. Guillard H, Murrone A. On the behaviour of upwind schemes in the low Mach number limit: II. Godunov type schemes. *Computers and Fluids* 2004; **33**:655–675.
22. Schneider Th, Botta N, Geratz K-J, Klein R. Extension of finite volume compressible flow solvers to multi-dimensional, variable density zero mach numberflow. *Journal of Computational Physics* 1999; **155**:248–286.
23. Lee SH. Convergence characteristics of preconditioned Euler Equations. *Journal of Computational Physics* 2005; **208**:266–288.
24. Hauke G, Hughes TJR. A comparative study of different sets of variables for solving compressible and incompressible flows. *Computer Methods in Applied Mechanics and Engineering* 1998; **153**:1–44.
25. Vigneron D, Deliége G, Essers JA. Low Mach number local preconditioning for unsteady viscous finite volumes simulations on 3D unstructured grids. *ECCOMAS Computational Fluid Dynamics Conference 2006*, TU Delft, Netherland, 2006; 1–14.
26. Turkel E. Preconditioned methods for solving incompressible and low speed compressible equations. *Journal of Computational Physics* 1987; **72**:277–298.
27. Roe PL. Characteristic based schemes for the Euler equations. *Annual Review of Fluid Mechanics* 1986; **18**: 337–365.
28. Roe PL. Approximate Riemann solvers, parameter vectors, and difference schemes. *Journal of Computational Physics* 1981; **43**:352–357.
29. Spiteri RJ, Ruuth SJ. A new class of optimal high-order strong-stability-preserving time discretization methods. *Technical Report CS-2001-01*, Acadaia University, Wolfville, Nova Scotia, Canada, 2001.

DOI: 10.1002/fld